

GAS-FLOW SWITCH RECOVERY EXPERIMENTS*

G. M. Molen, E. G. Ruf, J. M. Kuhlman
Departments of Electrical and Mechanical Engineering
Old Dominion University
Norfolk, VA 23508

and

J. S. Bernardes
Naval Surface Weapons Center
Dahlgren, VA 22448

Summary

Recovery experiments have been conducted with a flowing gas spark gap using a two-dimensional, converging-diverging nozzle geometry. A two-pulse thyatron circuit supplied 10 kV - 30 kV pulses to a 0.318 cm gap with a risetime of 10 μ s. The relative self-breakdown voltage was recorded as a function of the pulse separation and gas velocity.

The flow system consisted of a blow-down tunnel using air in which flow over the electrodes reached supersonic speeds at the higher total pressures. The flow field was characterized at several pressures by recording axial pressure distributions from which velocities were calculated. The spark gap recovery was found to be a strong function of the flow parameters especially at subsonic speeds where the recovery time was reduced to 0.15 ms as compared with 5.0 ms without flow.

Introduction

Spark gap recovery is critical to the performance of switches which are to be used at high repetition rates. Switch recovery characteristics have been addressed in this investigation using a spark gap which was mounted in a two-dimensional, converging-diverging nozzle that was affixed to a blow-down tunnel. Two identical high voltage pulses were applied to the gap with a variable time delay between the pulses. The voltage was applied using a circuit which had a rather long risetime ($\approx 10 \mu$ s), and the voltage at which the gap broke down was recorded for both pulses.

The voltage at which the first pulse broke down the gap is representative of the dielectric strength of the gap while the ratio of the second pulse to the first is defined as the recovery of the gap. This paper describes the recovery of this particular gap as the time between pulses is varied for three different gas flow conditions. The spatial location of the two arcs was also found to be a function of gas flow and the time between the pulses.

Pulsed Power Circuit

The pulsed power circuit used in the investigation is shown in Fig. 1. Two pulses were produced by identical circuits which connected to the gap and were independently triggered. A 0-30 kV DC power supply charged the two energy storage capacitors identified as C_1 through resistors R_0 and R_1 . Capacitor C_2 , which was placed across the spark gap, was considerably smaller than C_1 . Resistor R_3 was selected so that minimal voltage appeared across C_2 during the charging process.

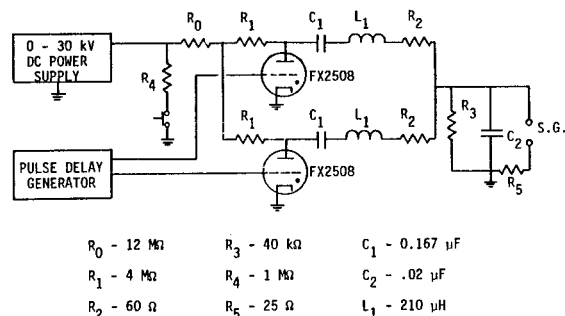


Fig. 1. Schematic of pulsed power circuit.

Voltage was applied to the spark gap when the first thyatron tube was triggered. In this process capacitor C_2 was resonantly charged to approximately 1.1 times the supply voltage. Because of the relative size of C_1 and C_2 , approximately 90% of the initial charge was left on C_1 . Resistor R_3 was of sufficient size so as to cause minimal damping. This scheme has been employed so as to apply voltage to the gap with approximately a $(1 - \cos \omega t)$ waveform and such that the peak voltage occurs at approximately 10 μ s. Once self-breakdown occurred, capacitor C_2 discharged through the gap and the circuit was critically damped by resistor R_5 . For a supply voltage of 20 kV, peak currents of 800 A were produced with a risetime of 0.25 μ s. This primary pulse was followed by a slower pulse which corresponded to the discharge of the energy remaining in C_1 . This slow pulse, which was close to critically damped by resistor R_2 , was approximately one-third the amplitude of the primary pulse and had a risetime of 7 μ s and a pulsewidth of 20 μ s.

Shown in Fig. 2(a) is a photograph of the voltage applied to the spark gap where the abrupt drop in the waveform corresponds to the breakdown of the gap. In Fig. 2(b) a burst of two pulses is shown separated in time by 7 ms. The behavior of the circuit for the second pulse was identical to the first except that the second thyatron was triggered. The switch recovery was established by comparing the relative amplitudes of these two pulses. In these photographs the voltage has been monitored by a high-voltage probe connected directly across the spark gap, and the waveform was displayed on a storage oscilloscope. A video camera was used to permanently record the oscilloscope traces so that the data could be analyzed at a later time. Using this data collection technique, the two-pulse bursts were repeated every 5 sec.

*Supported by Naval Surface Weapons Center under contract N60921-81-C-A221.

Report Documentation Page				Form Approved OMB No. 0704-0188	
Public reporting burden for the collection of information is estimated to average 1 hour per response, including the time for reviewing instructions, searching existing data sources, gathering and maintaining the data needed, and completing and reviewing the collection of information. Send comments regarding this burden estimate or any other aspect of this collection of information, including suggestions for reducing this burden, to Washington Headquarters Services, Directorate for Information Operations and Reports, 1215 Jefferson Davis Highway, Suite 1204, Arlington VA 22202-4302. Respondents should be aware that notwithstanding any other provision of law, no person shall be subject to a penalty for failing to comply with a collection of information if it does not display a currently valid OMB control number.					
1. REPORT DATE JUN 1983		2. REPORT TYPE N/A		3. DATES COVERED -	
4. TITLE AND SUBTITLE Gas-Flow Switch Recovery Experiments				5a. CONTRACT NUMBER	
				5b. GRANT NUMBER	
				5c. PROGRAM ELEMENT NUMBER	
6. AUTHOR(S)				5d. PROJECT NUMBER	
				5e. TASK NUMBER	
				5f. WORK UNIT NUMBER	
7. PERFORMING ORGANIZATION NAME(S) AND ADDRESS(ES) Departments of Electrical and Mechanical Engineering Old Dominion University Norfolk, VA 23508				8. PERFORMING ORGANIZATION REPORT NUMBER	
9. SPONSORING/MONITORING AGENCY NAME(S) AND ADDRESS(ES)				10. SPONSOR/MONITOR'S ACRONYM(S)	
				11. SPONSOR/MONITOR'S REPORT NUMBER(S)	
12. DISTRIBUTION/AVAILABILITY STATEMENT Approved for public release, distribution unlimited					
13. SUPPLEMENTARY NOTES See also ADM002371. 2013 IEEE Pulsed Power Conference, Digest of Technical Papers 1976-2013, and Abstracts of the 2013 IEEE International Conference on Plasma Science. Held in San Francisco, CA on 16-21 June 2013. U.S. Government or Federal Purpose Rights License.					
14. ABSTRACT					
15. SUBJECT TERMS					
16. SECURITY CLASSIFICATION OF:			17. LIMITATION OF ABSTRACT SAR	18. NUMBER OF PAGES 4	19a. NAME OF RESPONSIBLE PERSON
a. REPORT unclassified	b. ABSTRACT unclassified	c. THIS PAGE unclassified			

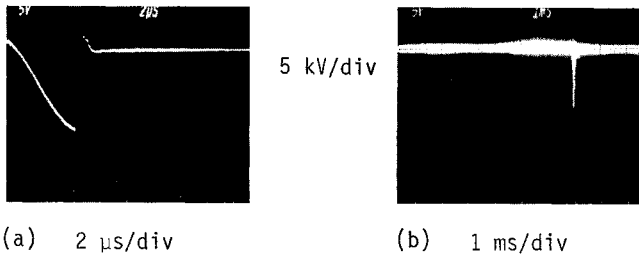


Fig. 2. Voltage applied to spark gap. In (a) waveform shown until breakdown and in (b) a two-pulse burst is shown with pulse separation of 7 ms.

Spark Gap Description

The spark gap flow channel used in the present study was designed as an insert to the test section of an existing, Aerolab 10 cm by 10 cm blow-down supersonic wind tunnel. A cross-sectional view of this flow channel is shown in Fig. 3. The flow channel consisted of an asymmetrical converging-diverging nozzle made of laminated Plexiglas. The upper wall of the spark gap flow channel could be pivoted to adjust the minimum separation of the nozzle, which will be referred to as the throat. Data presented herein for spark gap recovery and flow conditions were all obtained with a throat separation equal to $d = 0.318$ cm (0.125 in); the nozzle flow passage was 8.86 cm wide. Electrodes used in the present study were made of brass and were 2.54 cm wide. The electrodes were mounted on the centerline of the flow channel, and were contoured to match the Plexiglas nozzle contour. The electrodes were located at the throat and extended upstream and downstream of the throat as indicated in Fig. 4. The lower nozzle block was fitted with ten 0.102 cm ID static pressure orifices mounted flush to the wall at axial positions along the flow channel as indicated in Fig. 3. These static pressure taps were offset to one side of the channel centerline. Also, a total pressure probe was mounted on the opposite side of the flow channel at the same axial position as the first static pressure tap. These pressure taps were connected via plastic tubing to a manually operated scanning valve which was used to connect the pressure taps sequentially to a 0-45 psia (0-2330 torr) pressure gage. Also, the supersonic wind tunnel air supply pressure and temperature were monitored during all tests. A schlieren flow visualization system was available to visualize shock location in the spark gap flow channel.

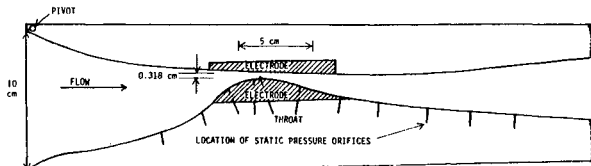


Fig. 3. Cross section of spark gap flow channel showing location of electrodes and pressure orifices.

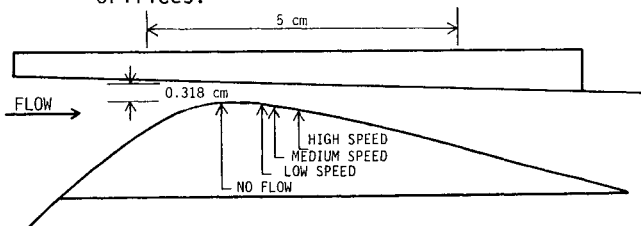


Fig. 4. Cross section of spark gap electrodes, showing location of first arc channel.

For each of the three flow conditions in the present study for which spark gap recovery data were obtained, a series of diagnostic measurements were made to characterize the flow in the spark gap. Flow conditions were essentially determined by the choice of air supply pressure in the wind tunnel plenum which was located upstream of the spark gap flow channel. This plenum supply pressure, called the total pressure, p_T , was held fixed during any single data run, and resulted in unique values of air flow rate, velocity, and axial pressure distributions for each value of p_T .

Generally, as p_T was increased, the velocity at a fixed axial location also increased. The pressure at the throat (the location of the minimum electrode separation) also increased somewhat, leading to a slight increase in self-breakdown voltage of the gap. For the three flow conditions for which spark gap recovery data were obtained (termed low, medium, and high speed), the axial static pressure distributions were measured. This enabled calculation of the axial distribution of the product of pressure times electrode separation, pd , using the measured channel geometry. Also, use of the $p(x)$ data allowed calculation of estimated average axial velocity distributions using one-dimensional gas dynamic theory.

The measured axial static pressure distributions in the spark gap are presented in Fig. 5 for the three flow conditions of low, medium, and high speed, corresponding to tunnel total pressures of 2.0, 7.8 and 16.8 psig, respectively (863, 1163, and 1629 torr). The axial static pressure data have been normalized by the absolute total pressure while the axial distance has been normalized by the minimum electrode separation, or throat dimension, of $d_{throat} = 0.318$ cm. The origin of the x-axis was chosen at the throat. These three conditions correspond to a flow which was completely subsonic for $p_T = 2.0$ psig (low speed), a flow which approached sonic speed at the nozzle throat for $p_T = 7.8$ psig (medium speed), and a flow in which a region of supersonic flow existed for $p_T = 16.8$ psig (high speed).

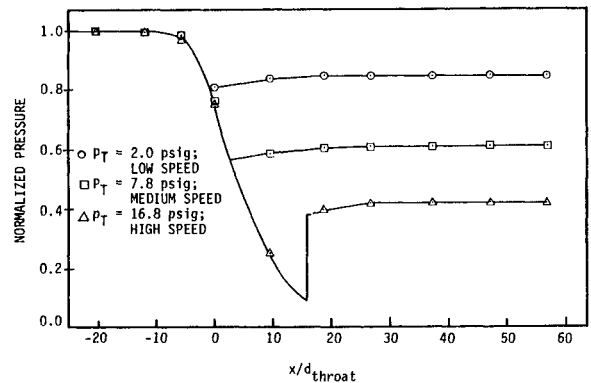


Fig. 5. Non-dimensional axial static pressure distribution for spark gap flow channel with electrode separation of $d_{throat} = 0.318$ cm.

These static pressure data have been found to match closely the $p(x)$ distributions obtained using one-dimensional gas dynamic theory up to axial positions where a shock occurred for the supersonic flow case or to axial positions where separation occurred in the diverging position of the nozzle for subsonic flow cases. However, the measured data were observed to be shifted slightly in the downstream direction as if the effective nozzle throat were displaced downstream of the

geometric throat. This was apparently due to growth of the nozzle wall boundary layers. It is noted that the indicated shock location for $p_T = 16.8$ psig, the high speed flow condition, has been estimated based upon these data and $p(x)$ data obtained at $p_T = 14.0$ and 20.0 psig which is not presented here. Although this shock has been shown as a normal shock in Fig. 5, it was observed in schlieren flow visualization studies that the actual shock was a two-dimensional structure. Thus, the actual $p(x)$ distribution averaged across the channel would have increased gradually with x between the fifth and sixth pressure taps for the high-speed flow condition.

The calculated axial distributions of the product of pressure times gap spacing (the pd product) are presented in Fig. 6 for the three previously described flow conditions. The nozzle geometry and the axial static pressure distributions presented in Fig. 5 have been used to compute these results. For the low and medium flow speeds ($p_T = 2.0$ and 7.8 psig, respectively) the minimum value of the pd product was found to occur at or just downstream of the nozzle throat, the point of minimum electrode separation. However, for the high speed flow ($p_T = 16.8$ psig) the minimum

value of the pd product clearly occurred downstream of the nozzle throat. This resulted because the pressure decreased more rapidly with axial position downstream of the throat than the area increased. The estimated axial location of this minimum pd product of $x \approx 10 d_{throat} \approx 3.18$ cm, was reasonably close to the observed axial position for the first arc, as indicated in Figure 4. The axial locations of the arc were determined utilizing video camera records of many shots for each flow condition. The locations of the first arc at the low and medium flow speeds were observed to occur upstream of the first arc location for the high speed flow. This observation was consistent with the location of the pd minimum shown in Fig. 6.

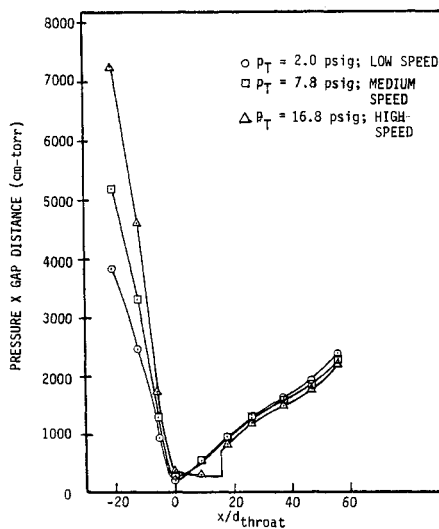


Fig. 6. Axial pressure-distance product distribution in spark gap flow channel for electrode separation of $d_{throat} = 0.318$ cm.

The computed average axial velocity distributions for the low, medium, and high flow speeds are presented in Fig. 7. These velocity results were calculated from the static pressure distributions (Fig. 5) for the appropriate total pressure and temperature using one-dimensional gas dynamic theory. The estimated velocity distribution of the shock for the high-speed flow ($p_T = 16.8$ psig), as indicated by the dashed curve,

was obtained using normal shock relations for the estimated shock location; hence, these results are relatively uncertain. It is noted that the average velocity is relatively constant in the diverging portion of the flow channel for all three flow speeds indicating that this diffuser section was separated. This flow separation has also been indicated in Fig. 5 by the lack of pressure recovery. The maximum calculated velocities were approximately 189 m/s (620 ft/s) for $p_T = 2.0$ psig, 293 m/s (960 ft/s) for $p_T = 7.8$ psig, and 427 m/s (1400 ft/s) for $p_T = 16.8$ psig. Calculated average velocities in the region between the first arc location and the downstream end of the top electrode (Fig. 4) were 180 m/s, 285 m/s, and 365 m/s, respectively. As mentioned previously, since the actual shock location, and hence the shock strength, for the high-speed flow condition was not known and since the actual shock structure was two dimensional, the actual axial velocity distribution for this flow condition would vary more smoothly with axial position in the vicinity of the shock.

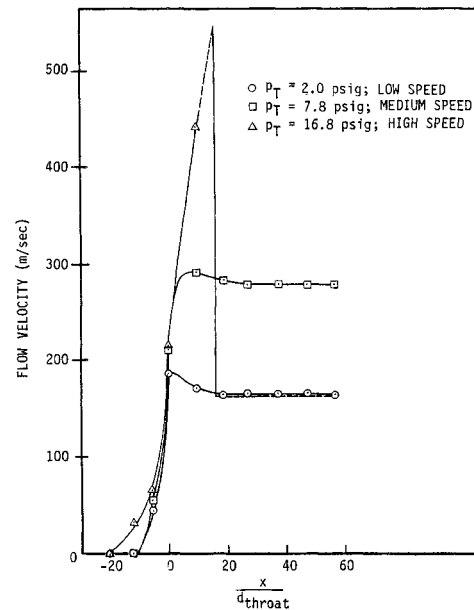


Fig. 7. Axial velocity distribution in spark gap flow channel for electrode separation of $d_{throat} = 0.318$ cm.

Experimental Results

Shown in Figs. 8 and 9 are recovery data for the three flow conditions identified as low, medium, and high speed as a function of the interpulse spacing. The actual breakdown voltage varied between 12 kV to 15 kV depending upon the spark gap pressure for each flow speed considered. Each data point shown in these figures corresponds to greater than 30 actual shots; error bars corresponding to one standard deviation are selectively shown to illustrate the observed spread in the data. In Fig. 8, the voltage recovery is shown for both low-speed flow and without flow at atmospheric pressure. A significant improvement in the gap recovery is noted between the two curves where the recovery time is observed to decrease from approximately 5 ms without flow to 0.2 ms with flow. The statistical variation with gas flow was considerably less than without flow for interpulse delays greater than 0.2 ms (knee of recovery curve). It is worthwhile to note that without gas flow the voltage recovery actually exceeded 100% for long delays suggesting that the first arc increased the dielectric strength of the gap in preparation for the second pulse. This effect was not observed with gas flow.

Experimental results similar to Fig. 8 are shown in Fig. 9 as the flow velocity is further increased corresponding to the medium and high speed. Comparing these results with the previous data, one may note that the knees of the curves are moved toward shorter delays as the speed is increased, much as one would anticipate. The droop in both curves for delays that extend past the knee of each curve is, however, rather surprising. Apparently the droop increases with flow velocity. After a careful analysis and with the use of diagnostics such as schlieren, the gradual degradation in the switch recovery appears to result from separation in the gas flow boundary layer downstream of the throat which increases with velocity.

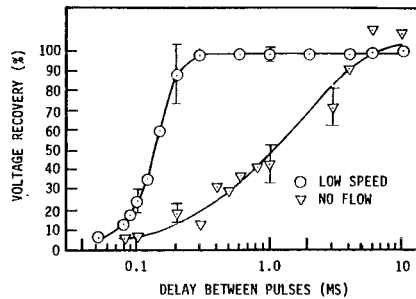


Fig. 8. Spark gap voltage recovery as a function of time delay between pulses without flow and for low speed flow.

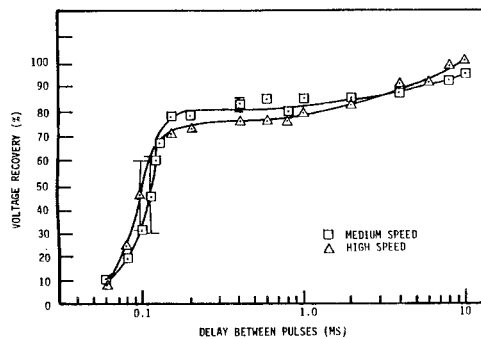


Fig. 9. Spark gap voltage recovery as a function of time delay between pulses for medium and high speed flow.

It was visually observed that the axial location of the second discharge was a function of the delay between the two pulses. The location of the first pulse has previously been correlated with the location of the minimum in the axial pd product distribution. The spatial separation between pulses is shown in Figs. 10 and 11 as a function of the interpulse delay for the three flow conditions. In all three cases, it is noted that the spatial separation drastically increases as the delay increases until the second arc has actually left the downstream end of the electrode. At such time, the second discharge again returns to the minimum pd product position.

For each flow condition, an estimate of the gas velocity in the arc region has been used to compute the distance that arc products would travel in the interval between the two pulses. These calculations are shown as solid curves in the two figures. It is seen that these curves are in fair agreement with the experimental data. It is interesting to compare the time delay at which the arc separation is dramatically reduced in Figs. 10 and 11 to the location of the knees of the recovery curves in Figs. 8 and 9. That these two delays were approximately equal implies that recovery for the spark gap occurred once the arc products

had been removed from the interelectrode region. It is significant that the arc separation for times greater than that required for the first arc products to clear the interelectrode region was essentially zero for the low speed case but became progressively larger for the medium and high speed cases. This observation substantiates the hypothesis that flow separation adversely affected the spark gap recovery at the high velocities.

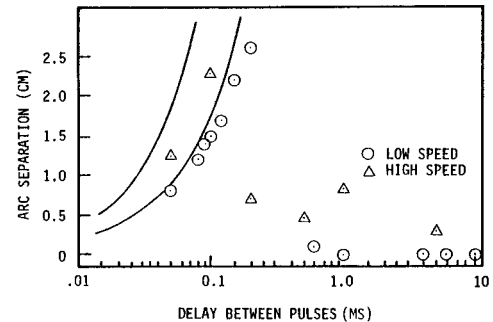


Fig. 10. Spatial displacement between pulses in bursts for low and high speed flow as a function of time delay between pulses.

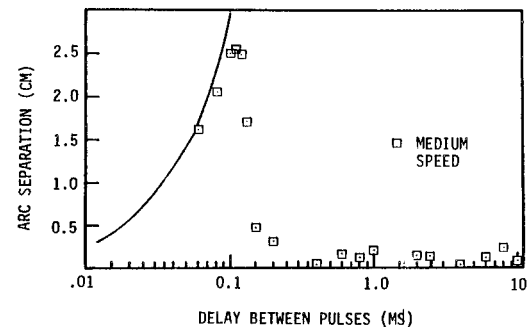


Fig. 11. Spatial displacement between pulses in bursts for medium speed flow as a function of time delay between the pulses.

Conclusions

It was experimentally observed that significant improvements in the recovery of a spark gap can result with uniform, laminar gas flow. Using electrodes that extended several centimeters in the direction of the flow, it was found that the second pulse would strike through the arc debris produced by the first pulse until such time that the debris was completely removed from the electrode region. At that time, the dielectric strength of the gap was completely restored, at least for the low speed case. For higher flow speeds, a droop in the gap recovery was measured and schlieren visualization of the flow channel suggests that it resulted from separation of the boundary layer